Atmos. Chem. Phys., 13, 531–545, 2013
www.atmos-chem-phys.net/13/531/2013/
doi:10.5194/acp-13-531-2013


Atmospheric Chemistry and Physics

# Wavelength and $NO_x$ dependent complex refractive index of SOAs generated from the photooxidation of toluene

**T. Nakayama**[1], **K. Sato**[2], **Y. Matsumi**[1], **T. Imamura**[2], **A. Yamazaki**[2], **and A. Uchiyama**[3]

[1]Solar-Terrestrial Environment Laboratory and Graduate School of Science, Nagoya University, Furo-cho, Chikusa-ku, Nagoya 464-8601, Japan
[2]National Institute for Environmental Studies, 16-2, Onogawa, Tsukuba 305-8506, Japan
[3]Meteorological Research Institute, Japan Meteorological Agency, 1-1, Nagamine, Tsukuba 305-0052, Japan

*Correspondence to:* T. Nakayama (nakayama@stelab.nagoya-u.ac.jp)

Received: 6 April 2012 – Published in Atmos. Chem. Phys. Discuss.: 8 June 2012
Revised: 22 December 2012 – Accepted: 2 January 2013 – Published: 16 January 2013

**Abstract.** Recently, secondary organic aerosols (SOAs) generated from anthropogenic volatile organic compounds have been proposed as a possible source of light-absorbing organic compounds, "brown carbon," in the urban atmosphere. However, the atmospheric importance of these SOAs remains unclear due to limited information about their optical properties. In this study, the complex refractive index (RI, $m = n$-$ki$) values at 405, 532, and 781 nm of the SOAs generated during the photooxidation of toluene (toluene-SOAs) under a variety of initial nitrogen oxide ($NO_x = NO + NO_2$) conditions were examined by photoacoustic spectroscopy (PAS) and cavity ring-down spectroscopy (CRDS). The complex RI-values obtained in the present study and reported in the literature indicate that the $k$-value, which represents the light absorption of the toluene-SOAs, increased to shorter wavelengths at $<532$ nm, and the $n$-value also increased to shorter wavelengths from 781 to 355 nm. The $k$-values at 405 nm were found to increase from 0.0018 to 0.0072 with increasing initial $NO_x$ concentration from 109 to 571 ppbv. The nitrate to organics ratio of the SOAs determined using a high-resolution time-of-flight aerosol mass spectrometer (H-ToF-AMS) also increased with increasing initial $NO_x$ concentration. The RI-values of the SOAs generated during the photooxidation of 1,3,5-trimethylbenzene in the presence of $NO_x$ (1,3,5-TMB-SOAs) were also determined to investigate the influence of the chemical structure of the precursor on the optical properties of the SOAs, and it was found that the light absorption of the 1,3,5-TMB-SOAs is negligible at all of the wavelengths investigated (405, 532, and 781 nm). These results can be reasonably explained by the hypothesis that nitroaromatic compounds, such as nitrocresols, are the major contributors to the light absorption of the toluene-SOAs. Using the obtained RI-values, mass absorption cross sections of the toluene-SOAs at 405 nm were estimated to be 0.08–0.52 $m^2 g^{-1}$ under typical conditions in an urban atmosphere during the daytime. These results indicate that light absorption by the SOAs potentially contributes to the radiation balance at ultraviolet wavelengths below ∼400 nm, specifically when the mass concentrations of the anthropogenic SOAs are significant compared with other light-absorbing particles.

## 1 Introduction

Atmospheric aerosol plays an important role in determining the visibility, health effects, heterogeneous chemistry, and radiation balance of the atmosphere on a local and a global scale (Seinfeld and Pandis, 2006; Finlayson-Pitts and Pitts, 2000). Recently, it has been suggested that the organic aerosols called "brown carbon" can absorb solar radiation, especially at ultraviolet (UV) and shorter visible wavelengths, and contribute to the radiation balance and photochemical reactions in the atmosphere (Andreae and Gelencsér 2006; Moosmüller et al., 2009; Alexander et al., 2008 and references therein). "Brown carbon" is operationally defined as a light-absorbing carbonaceous material with a wavelength dependent imaginary part ($k$) of the complex refractive index (RI), $m = n - ki$.

Sources of brown carbon have been reported to be the organic components generated during the combustion of

biomass, such as wood (Kirchsteller et al., 2004; Chen and Bond, 2010), corn stem (Schnaiter et al., 2005), and rice straw (Faves et al., 2009), as well as fossil fuels, such as propane (Schnaiter et al., 2006), coal (Bond 2001), and the organic components included in diesel exhaust (Adler et al., 2010). Humic-like substances (HULIS) extracted from aerosols generated by biomass burning (Hoffer et al. 2006) and sampled in air pollution, rural forests, and fresh smoke conditions (Dinar et al., 2008) were also reported to exhibit light absorption, especially at UV and shorter visible wavelengths.

Secondary organic aerosols (SOAs) contain many different chemicals including high molecular weight products, and thus may possibly act as "brown carbon" (Graber and Rudich, 2006; Hallquist et al., 2009). Jacobson (1999) suggested the possible influence of the near UV light absorption by nitrated and aromatic aerosol components on reductions in downward solar radiation in the Los Angeles region. Recently, SOAs generated during the gas-phase photooxidation of toluene in the presence of nitrogen oxides ($NO_x = NO + NO_2$) (Jaoui et al., 2008; Nakayama et al., 2010a; Zhong and Jang, 2011), the chemical aging of SOAs generated from the reaction of *d*-limonene with $O_3$ (Bones et al., 2010; Laskin et al., 2010), the irradiation of aqueous solutions containing $H_2O_2$ and phenolic compounds (Chang and Thompson; 2010), and aqueous phase reactions involving glyoxal and methyglyoxal (Shapiro et al., 2009; Galloway et al., 2009; Sareen et al., 2010; Trainic et al., 2011) were reported to exhibit light absorption at UV and/or shorter visible wavelengths.

The photooxidation of aromatic hydrocarbons such as toluene, xylene, and trimethylbenzene (TMB) in the presence of $NO_x$ is known as a major source of anthropogenic SOAs (Kleindienst et al., 2004; Ng et al., 2007; Henze et al., 2008); therefore, quantitative characterization of the optical properties of these SOAs is required in order to estimate the effect of anthropogenic SOAs on the atmospheric radiation balance. However, only a few experimental studies on the determinations of the RI-values of light-absorbing SOAs have been reported. Kim et al. (2010) reported the real part of the RI at 670 nm for the SOAs generated during the photooxidation of toluene in the presence of $NO_x$ (denoted by toluene-SOAs) under a variety of initial hydrocarbon ($[HC]_{ini} =$ 1.71-3.75 ppmv) and $NO_x$ ($[NO_x]_{ini} = 820$–$3100$ ppbv) conditions in the absence of seed particles, and reported *n*-values ranging from 1.4 to 1.6 using a polar nephelometer. Our group (Nakayama et al., 2010a) retrieved the real and imaginary parts of the RI-values at 355 and 532 nm for the toluene-SOAs generated in the presence of $[HC]_{ini} = 4.0$ ppmv and $[NO_x]_{ini} = 540$ ppbv in the absence of seed particles by measuring the extinction and scattering coefficients using a cavity ring-down spectrometer (CRDS) and a nephelometer, respectively. The RI-values of $m = (1.632^{+0.038}_{-0.035}) - (0.047^{+0.041}_{-0.036})i$ at 355 nm and $m = (1.483^{+0.032}_{-0.036}) - (0.007^{+0.030}_{-0.007})i$ at 532 nm were reported. A non-negligible *k*-value was obtained at 355 nm, while no evidence of light absorption was found at 532 nm due to the difficulty of quantifying the small difference between the extinction and scattering coefficients. Therefore, direct measurement of the absorption coefficients is desired for the accurate determination of small *k*-values. Zhong and Jang (2011) measured the absorption spectrum of toluene-SOAs that were generated with and without seed particles using a UV-visible spectrometer with an integrating sphere after collection on a filter. Based on the absorption spectrum, they reported the imaginary part of the RI-value at 350 nm for the toluene-SOAs generated in the presence of $[HC]_{ini} = 0.207$ and 0.202 ppmv and $[NO_x]_{ini} = 62$ and 70 ppbv in the absence of seed particles to be $k = 0.0214$ and 0.0215. They also reported that the SOAs generated in the presence of $(NH_4)_2SO_4$ or $NH_4HSO_4$+$H_2SO_4$ (1:1 molar mixture) seed particles have *k*-values that are 2–3 times larger at 350 nm than those generated in the absence of seed particles. Nitrated aromatic compounds such as nitrocresols were considered as plausible sources of the light absorption observed by Nakayama et al. (2010a) and Zhong and Jang (2011). The production quantum yield of nitrated aromatic compounds may depend on $[NO_x]_{ini}$,; however, the *k*-values were measured under limited $[NO_x]_{ini}$ conditions: 540 ppbv (Nakayama et al., 2010a) and 62–70 ppbv (Zhong and Jang, 2011).

Herein, results of the detailed investigation of the wavelength and $NO_x$ dependence of the complex RI-values of toluene-SOAs are presented. To determine the small *k*-value accurately, a 3λ-photoacoustic spectrometer (Droplet Measurement Technologies, PASS-3) was used to directly measure the light absorption of the SOAs suspended in air. In addition, the complex RI-values of the SOAs generated during the photooxidation of 1,3,5-TMB in the presence of $NO_x$ (denoted by 1,3,5-TMB-SOAs) were also determined to investigate the influence of chemical structure on the optical properties of SOAs generated from aromatic hydrocarbons. Using the obtained RI-values, possible atmospheric implications of the light absorption of the anthropogenic SOAs are also discussed.

## 2 Experimental

The experimental setup used in this study, which is shown in Fig. 1, is similar to that used in our previous study (Nakayama et al., 2010a, 2012). The SOAs were generated in a 6 $m^3$ Teflon-coated stainless steel photochemical smog chamber (Akimoto et al., 1979; Sato et al., 2007). The toluene (or 1,3,5-TMB), NO, methyl nitrate, and purified air were mixed in the chamber and continuously irradiated by light from a xenon arc lamp (19 kW) through Pyrex filters. Methyl nitrite (∼0.01 ppmv) was used as the OH source. Toluene (Wako Chemicals, 99 %), 1,3,5-TMB (Tokyo Chemical Industry, >97 %), and NO (Takachiho

**Table 1.** Experimental conditions, mass concentrations, and surface mean diameters of the SOAs used for determination of the RI-values.

| Run[a] | Compounds | $[HC]^b_{ini}$ (ppmv) | $[NO_x]^b_{ini}$ (ppbv) | $M_p^c$ ($\mu g\,m^{-3}$) | $\bar{D}_s^d$ (nm) |
|---|---|---|---|---|---|
| A1 | Toluene | 3.9 | 109 | 31–34 | 133–149 |
| A2 | Toluene | 3.9 | 167 | 40–60 | 119–170 |
| A3 | Toluene | 4.0 | 289 | 81–113 | 153–218 |
| A4 | Toluene | 4.0 | 571 | 119–160 | 211–270 |
| B1 | 1,3,5-TMB | 2.4 | 571 | 78–117 | 370–429 |

[a] No seed particles were added in the present study.
[b] NO was used for all experimental runs.
[c] Range of mass concentrations of the SOAs estimated from the size distributions measured by the SMPS assuming a particle density of 1.4 g $cm^{-3}$(Sato et al., 2007). Effects of dilution and wall loss were not taken into account.
[d] Range of surface mean diameters of the SOAs measured by the SMPS.

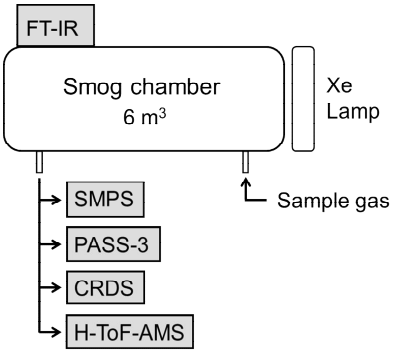


**Fig. 1.** Schematic diagram of the experimental setup; SMPS, scanning mobility particle sizer; PASS-3, 3λ-photoacoustic soot spectrometer; CRDS, cavity ring-down spectrometer; FT-IR, Fourier transform-infrared spectrometer; H-ToF-AMS, high-resolution time-of-flight aerosol mass spectrometer.

Chemical Industrial Co., 99.9 %) were used without further purification. No seed particles were added in the present study. The total pressure in the chamber was maintained at 1000-1030 hPa by adding purified air during the measurements. All experiments were conducted under room temperature (298 ± 3 K) and dry ($[H_2O]$ <1 ppmv) conditions. Four experiments (runs A1–A4) were conducted for the toluene-SOAs with different $[NO_x]_{ini}$ conditions (109–571 ppbv) in order to examine the $NO_x$ dependence of the RI-values, as shown in Table 1. In addition, one experiment (run B1) was conducted for the 1,3,5-TMB-SOAs with a high $[NO_x]_{ini}$ condition (571 ppbv).

The concentrations of toluene, 1,3,5-TMB, NO, $NO_2$, and $O_3$ were monitored using a Fourier transform infrared spectrometer (FT-IR; Nicolet, Nexus 670) combined with a mirror system with a 221.5 m optical path. The particle size distribution was measured every 6 min using a scanning mobility particle sizer (SMPS; TSI, 3934). Typical temporal profiles of the toluene, NO, $NO_2$, $O_3$, mass concentrations, and the surface mean diameters of the toluene-SOAs during "run A4" are shown in Fig. 2. When the mass concentration of the SOAs began to increase, the SOAs were introduced into the PASS-3 and a custom-built CRDS.

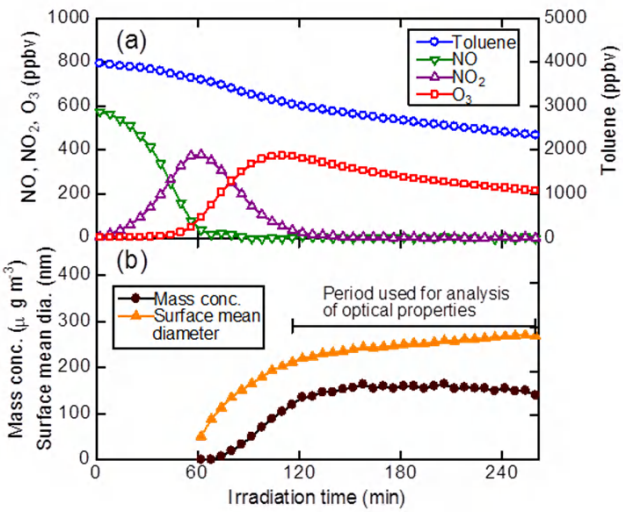


**Fig. 2.** Temporal profiles of (a) toluene (open circles), NO (open inverted triangles), $NO_2$(open triangles), and $O_3$ (open squares), and **(b)** mass concentrations (filled circles) and surface mean diameters (filled triangles) during "run A4". The bar indicates the period used for analysis of the optical properties.

The PASS-3 instrument was used to measure the absorption ($b_{abs}(\lambda)$) and scattering ($b_{sca}(\lambda)$) coefficients at 405, 532, and 781 nm. The $b_{sca}(\lambda)$ data were calibrated using monodisperse polystyrene latex (PSL) particles. The $b_{abs}$(405, 781 nm) data were calibrated using polydisperse propane soot particles, while the $b_{abs}$(532 nm) data were calibrated with monodisperse nigrosin particles and gaseous $NO_2$. These calibration procedures are described in the Supplemental Material (S1). The $b_{sca}$(532 nm) data obtained using the PASS-3 were not used in this study, because a strong particle size dependence of the calibration factors was found. Uncertainties associated with the calibration were estimated to be 8, 10, 8, 10, and 10 % for $b_{abs}$(405 nm), $b_{abs}$(532 nm), $b_{abs}$(781 nm), $b_{sca}$(405 nm), and $b_{sca}$(781 nm), respectively. For background interpolation, measurements of filtered air were conducted using a particulate filter (Balston), typically for 4 min every 12 min. The typical detection limits for the 12 min averaged data of $b_{abs}$(405 nm), $b_{abs}$(532 nm), $b_{abs}$(781 nm), $b_{sca}$(405 nm), and $b_{sca}$(781 nm) were estimated to be 1.0, 0.9, 0.4, 0.2, and 0.2 $Mm^{-1}$, respectively, by taking the two standard deviations ($2\sigma$) of each signal during the filtered air measurements. It should be noted that these detection limits varied depending on the magnitude of the drift in each signal. Corrections of $b_{abs}$ for the gas phase absorption of $NO_2$ were conducted using the mixing ratio measured via FT-IR, the absorption cross section, and the transmission of $NO_2$ through the particulate filter. Overall uncertainties for the PASS-3 data were estimated by taking into account

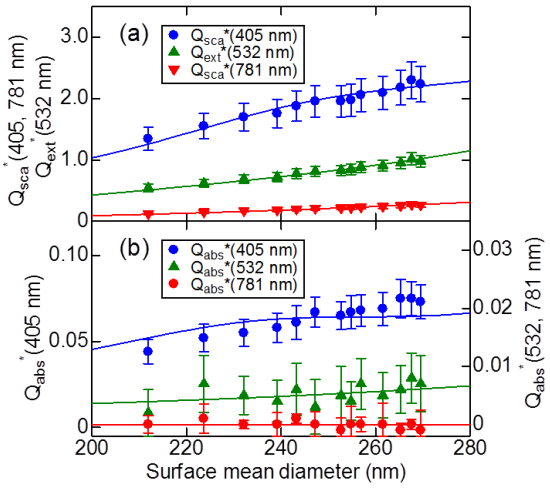


**Fig. 3.** Dependence of the effective **(a)** scattering (or extinction) and **(b)** absorption efficiencies of the polydisperse SOA particles on the surface mean diameter at wavelengths of 405 (circles), 532 (triangles), and 781 nm (inverted triangles) for the toluene-SOAs generated in "run A4". Error bars indicate the estimated uncertainties for the determination of the $Q_{sca}$* (or $Q_{ext}$*) and $Q_{abs}$* values. The solid lines indicate $Q_{sca}$* (or $Q_{ext}$*) and $Q_{abs}$* calculated using Mie theory with the optimized RI-values. The definitions of $Q_{sca}$*, $Q_{ext}$*, and $Q_{abs}$* are stated in the text.

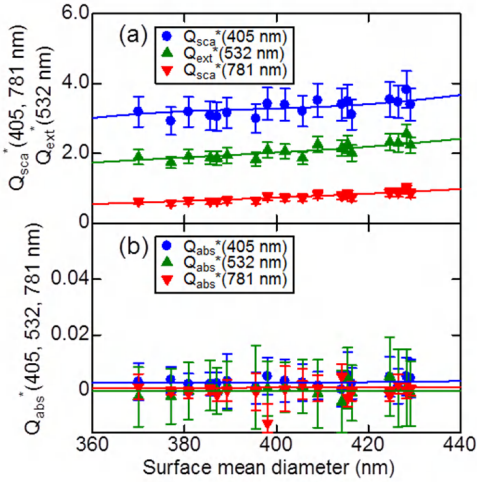


**Fig. 4.** Dependence of the effective **(a)** scattering (or extinction) and **(b)** absorption efficiencies of the polydisperse SOA particles on the surface mean diameter at wavelengths of 405 (circles), 532 (triangles), and 781 nm (inverted triangles) for the 1,3,5-TMB-SOAs generated in "run B1". The symbols are the same as those used in Fig. 3.

the uncertainties in the calibration factors, in the background interpolations (estimated from the drift between neighboring filtered air measurements), and in the corrections of the gas phase absorption, as well as the detection limit values. The sampling flow rate of the PASS-3 was 1.0 lpm.

The CRDS instrument was used to measure the extinction coefficients at 532 nm ($b_{ext}$(532 nm)). A detailed description of the CRDS instrument used in the present study is included in our previous papers (Nakayama et al., 2010a, b). Measurement of the ring-down time for the filtered air was conducted using a particulate filter (Pall), typically for 4 min every 12 min. A typical detection limit for the 12 min averaged data for $b_{ext}$(532 nm) during the experiments was estimated to be 0.06 $Mm^{-1}$ by taking the $2\sigma$ of each signal during the filtered air measurements. The accuracy and precision of the CRDS instrument were checked using monodisperse PSL particles, and the uncertainty in the determination of $b_{ext}$(532 nm) was estimated to be <5 %. The sampling flow rate of the CRDS was 0.7 lpm.

The chemical properties of the aerosols were also measured every 6 min using an Aerodyne aerosol mass spectrometer (Aerodyne Research, H-ToF-AMS) in the V-mode (Drewnick et al., 2005). The particles collected through an aerodynamic lens were heated at 873 K to evaporate the particulate compounds, and the vaporized compounds were then ionized by electron ionization and analyzed using a ToF-MS instrument with a mass resolution of ~2700. The data obtained via H-ToF-AMS were numerically analyzed using the ToF-AMS Analysis Toolkit program Version 1.48 combined with the ToF-AMS HR Analysis Program Version 1.07.

## 3 Results

The complex RI of the SOAs was determined using the same procedure that was used in our previous study (Nakayama et al., 2010a). Assuming homogeneous spherical particles, the effective absorption ($Q_{abs}$*($\bar{D}_s$, λ)), scattering ($Q_{sca}$*($\bar{D}_s$, λ)), and extinction ($Q_{ext}$*($\bar{D}_s$, λ)) efficiencies of polydisperse SOA particles with a surface mean diameter $\bar{D}_s$ at wavelength λ (=405, 532, or 781 nm) were calculated as follows:

$$Q^*_{abs,sca,ext}(\bar{D}_s, \lambda) = b_{abs,sca,ext}(\lambda) / \int N(D_p) \frac{\pi}{4} D_p^2 dD_p, \quad (1)$$

where $D_p$ is the geometrical particle diameter and $N$ is the number concentration of particles in the size bin $dD_p$ with a mean diameter $D_p$ per unit volume.

A 12-min average of the $b_{abs}$(405, 532, 781 nm), $b_{sca}$(405, 781 nm), and $b_{ext}$(532 nm) obtained with the PASS-3 and CRDS, and the size distributions obtained with the SMPS were used for the analysis. The range of $b_{abs}$, $b_{sca}$, and $b_{ext}$ values used for the determination of the RI-values is listed in Table 2. Figures 3 and 4 show the $Q_{abs}$* at 405, 532, and 781 nm, the $Q_{sca}$* at 405 and 781 nm, and the $Q_{ext}$ at 532 nm for "run A4" (toluene-SOAs, high $[NO_x]_{ini}$ condition) and "run B1" (1,3,5-TMB–SOAs, high $[NO_x]_{ini}$ condition), respectively, as a function of $\bar{D}_s$. Significant light absorption at 405 nm and non-negligible light absorption at 532 nm were found for "run A4" (Fig. 3b). In contrast, no significant light

**Table 2.** Absorption, scattering, and extinction coefficients used for the analyses and the RI-values determined in the present study.

| Run | λ (nm) | $b_{abs}^{a}$ ($Mm^{-1}$) | $b_{sca}$ or $b_{ext}^{b}$ ($Mm^{-1}$) | Refractive index ($m = n$-$ki$) | |
|---|---|---|---|---|---|
| | | | | $n$ | $k$ |
| A1 | 405 | 1.1–2.9 | 61.2–71.8 | $1.449^{+0.030}_{-0.030}$ | $0.0018^{+0.0013}_{-0.0014}$ |
| | 532 | <0.8 | 22.1–27.3 | $1.431^{+0.025}_{-0.026}$ | $0.0000^{+0.0029}_{-0.0000}$ |
| | 781 | <0.6 | 4.4–6.1 | $1.389^{+0.053}_{-0.056}$ | $0.0000^{+0.0018}_{-0.0000}$ |
| A2 | 405 | 2.0–5.3 | 67.5–166.5 | $1.467^{+0.029}_{-0.032}$ | $0.0030^{+0.0010}_{-0.0010}$ |
| | 532 | <2.1 | 26.2–70.5 | $1.457^{+0.025}_{-0.023}$ | $0.0004^{+0.0016}_{-0.0004}$ |
| | 781 | <1.9 | 4.5–14.5 | $1.403^{+0.036}_{-0.039}$ | $0.0000^{+0.0021}_{-0.0000}$ |
| A3 | 405 | 6.7–10.8 | 247.5–411.4 | $1.468^{+0.029}_{-0.031}$ | $0.0036^{+0.0007}_{-0.0007}$ |
| | 532 | <1.9 | 101.5–180.8 | $1.447^{+0.026}_{-0.028}$ | $0.0003^{+0.0010}_{-0.0003}$ |
| | 781 | <0.4 | 21.6–41.5 | $1.387^{+0.028}_{-0.029}$ | $0.0000^{+0.0006}_{-0.0000}$ |
| A4 | 405 | 24.8–43.0 | 762.8-1263.3 | $1.567^{+0.042}_{-0.043}$ | $0.0072^{+0.0010}_{-0.0010}$ |
| | 532 | 1.2–4.0 | 454.2–546.8 | $1.498^{+0.024}_{-0.025}$ | $0.0010^{+0.0007}_{-0.0008}$ |
| | 781 | <0.8 | 72.1–146.7 | $1.452^{+0.031}_{-0.030}$ | $0.0000^{+0.0006}_{-0.0000}$ |
| B1 | 405 | <1.3 | 722.2–953.5 | $1.485^{+0.062}_{-0.054}$ | $0.0002^{+0.0004}_{-0.0002}$ |
| | 532 | <1.1 | 529.3–679.3 | $1.459^{+0.028}_{-0.029}$ | $0.0000^{+0.0010}_{-0.0000}$ |
| | 781 | <1.3 | 186.8–191.0 | $1.423^{+0.028}_{-0.027}$ | $0.0002^{+0.0007}_{-0.0002}$ |

[a] Ranges of the absorption coefficients at 405, 532, and 781 nm measured using the PASS-3 instrument (12 min average).
[b] Ranges of the scattering coefficients at 405 and 781 nm, and those of the extinction coefficients at 532 nm measured using the PASS-3 and CRDS instruments, respectively (12 min average).

absorption was detected at all wavelengths (405, 532, and 781 nm) in "run B1" within the uncertainties (Fig. 4b).

The effective absorption, scattering, and extinction efficiencies can also be calculated using Mie theory as follows:

$$Q^*_{abs,sca,ext}(\bar{D}_s, \lambda) = \int f(D_p) Q_{abs,sca,ext}(D_p, \lambda) dD_p, \quad (2)$$

where $f(D_p)$ is the surface area weighted size distribution function normalized to the total surface area, and this calculation was carried out with the SMPS data. $Q_{abs,sca,ext}(D_p, \lambda)$ represent the absorption, scattering, and extinction efficiencies, and were calculated based on Mie theory using the BHMIE algorithm (Bohren and Huffman, 1983).

In this study, the optimized RI-values were determined using combinations of the data: (1) $Q^*_{sca}$ and $Q^*_{abs}$ at 405 and 781 nm and (2) $Q^*_{ext}$ and $Q^*_{abs}$ at 532 nm. To minimize the sum of the squared residual between the $Q^*$ values obtained using Eq. (1) and those obtained using Eq. (2), the optimized RI-value was determined. The $n$-value was fixed between 1.2 and 1.7 and a positive value of $k$ was chosen during the fitting procedure. The complex RI-value was determined for each experimental run by assuming a constant RI-value during the measurement. The results for $Q^*_{abs}$, $Q^*_{sca}$, and $Q^*_{ext}$ calculated using Eq. (2) with the optimized RI-values for "run A4" and "run B1" are shown as solid lines in Figs. 3 and 4, respectively. The obtained RI-values and their uncertainties, which were estimated from the $2\sigma$ for the differences between the $Q^*(\bar{D}_s, \lambda)$ values obtained using Eqs. (1) and (2) and the uncertainties in the measurements of the optical properties and size distributions of the SOAs, are summarized in Table 2. The uncertainties in the size distribution measurements were estimated to be <8 % based on the estimated total counting uncertainties (<5 %) and the uncertainties in the diameters of the PSL particles used for the calibration of the SMPS (<3 %). The total counting uncertainties were estimated by doubling the uncertainties obtained in the inspection of verification standards by the manufacturer. Milles et al. (2010) reported that the uncertainties in the particle size and RI of PSL particles, used for the calibration of a CRDS instrument, contributed to the uncertainties in the retrieved RI of other aerosols. In the present study, the uncertainties in the diameters of the PSL particles used for the calibration of the CRDS and PASS-3 were also taken into account in the estimation of the uncertainties for these instruments. The uncertainties in the determination of the $n$- and $k$-values actually varied, partly due to the differences in the abundance of the SOAs, and partly due to the drift in the absorption and scattering signals for each experimental run.

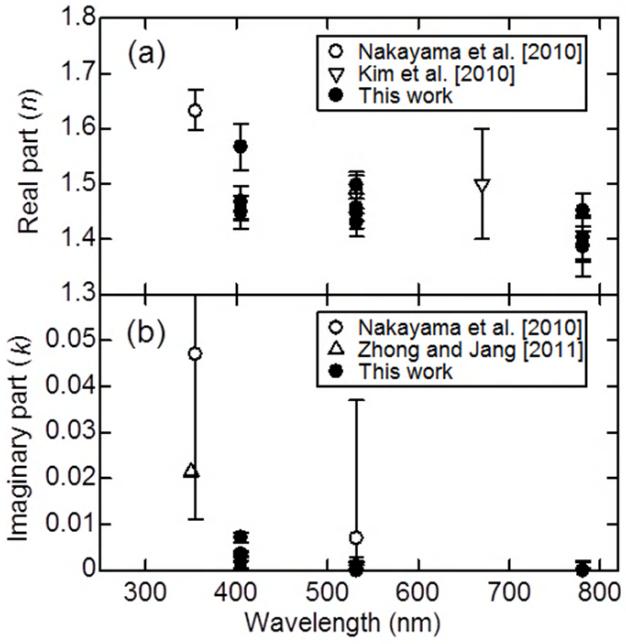


**Fig. 5.** Wavelength dependence of the **(a)** real and **(b)** imaginary parts of the RI-values for the toluene-SOAs determined in the present study and reported in the literature (Nakayama et al., 2010a; Kim et al., 2010; Zhong and Jang 2011).

## 4 Discussion

### 4.1 Wavelength dependence of the RI-values for toluene-SOAs

Figure 5 shows the wavelength dependence of the $n$ and $k$-values for the toluene-SOAs obtained in the present study ($n$ and $k$, runs A1–A4, filled circles) and reported in the literature, Nakayama et al. (2010a) ($n$ and $k$, open circles), Kim et al. (2010) ($n$, open inverted triangle), and Zhong and Jang (2011) ($k$, open triangle).

The $n$ values at 405, 532, and 781 nm obtained in the present study range between 1.4 and 1.6, and show an increase to shorter wavelengths. The $n$-value of $1.498^{+0.015}_{-0.014}$ at 532 nm under the high $[NO_x]_{ini}$ condition ($[NO_x]_{ini}$ = 571 ppbv, run A4) is in good agreement with that obtained in our previous study ($1.483^{+0.032}_{-0.036}$) (Nakayama et al., 2010a) under a high $[NO_x]_{ini}$ condition ($[NO_x]_{ini}$ = 540 ppbv). Interpolation of all of our results at 532 and 781 nm gives an $n$-value of ∼1.43 at 670 nm, which lies in the lower part of the range between 1.4 and 1.6 that was reported by Kim et al. (2010) for a variety of $[HC]_{ini}$ and $[NO_x]_{ini}$ conditions ($[HC]_{ini}$ = 1.71–3.75 ppmv, $[NO_x]_{ini}$ = 820–3100 ppbv). These results may be explained by their use of higher $[NO_x]_{ini}$ conditions than those of the present study.

Significant $k$ values at 405 nm, which range from $0.0018^{+0.0013}_{-0.0014}$ to $0.0072^{+0.0010}_{-0.0010}$, were obtained for the toluene-SOAs in the present study. The $k$-value depends on $[NO_x]_{ini}$, as discussed in detail in the next section. At 532 nm, the $k$-value of $0.0010^{+0.0007}_{-0.0008}$ obtained under high $[NO_x]_{ini}$ conditions (run A4) was slightly larger than the estimated uncertainties for this run, while the values for the other runs (A1, A2, and A3) are negligible within the experimental uncertainties for each run. At 781 nm, the $k$-values were found to be negligible for all runs. In our previous study (Nakayama et al., 2010a), the RI-values were determined from the measurements of the extinction and scattering coefficients. Therefore, precise determination of a small $k$-value was difficult because of the large uncertainties (typically ∼0.04), as shown by the larger error bars in Fig. 5b. In the present study, by directly measuring the absorption coefficients using the PASS-3, the $k$ values could be determined with a higher precision (typical uncertainties of ∼0.001).

The $k$-values obtained in the present study and reported in the literature (Nakayama et al., 2010a; Zhong and Jang 2011) suggest the existence of a resonance wavelength at shorter wavelengths. For a light-absorbing material, the $n$-value principally has a normal dispersion (i.e., $n$ decreases with increasing wavelength) for wavelengths well above the resonance wavelength. Thus, the observed features of the wavelength dependence of the $n$- and $k$-values are qualitatively consistent with the theoretically predicted features, if the absorption peak (resonant wavelength) is assumed to be shorter than 350 nm (e.g., Moosmüller et al., 2011).

### 4.2 $NO_x$ dependence of the RI-values for toluene-SOAs

Figure 6a and b show the $[NO_x]_{ini}$ dependence of the $n$ and $k$-values at 405 nm (filled circles) and 532 nm (open circles) for the toluene-SOAs obtained in the present study.

The $n$-values at 405 and 532 nm slightly increased from 1.45 to 1.57 and 1.43 to 1.50, respectively, with increasing $[NO_x]_{ini}$ from 109 to 571 ppbv, as shown in Fig. 6a. The difference in the $n$-values at 405 and 532 nm also increased from ∼0.02 to ∼0.07 with increasing $[NO_x]_{ini}$. These results are again consistent with the theoretically predicted features when the light absorption of a shorter resonant wavelength is taken into account (e.g., Moosmüller et al. 2011), because the stronger light absorption under high $[NO_x]_{ini}$ conditions would cause a larger increase in the $n$-values at 405 nm than at 532 nm. It should be noted that a change in chemical properties, such as the O/C ratio, may also contribute to the observed $[NO_x]_{ini}$ dependence of the $n$-values; a positive correlation has been reported for squalane and azelaic acid by Cappa et al.(2011).

At 405 nm, the $k$-values increase from 0.0018 to 0.0072 with increasing $[NO_x]_{ini}$ from 109 to 571 ppbv, as shown in Fig. 6b. The difference in the $k$-values at ∼350 nm reported by Nakayama et al. (2010a) and Zhong and Jang (2011) may be explained by the difference in the $[NO_x]_{ini}$ conditions: 540 ppbv (Nakayama et al., 2010a) and 62–70 ppbv (Zhong and Jang, 2011). At 532 nm, the $k$-value was slightly larger than the uncertainties under the high $[NO_x]_{ini}$ condition

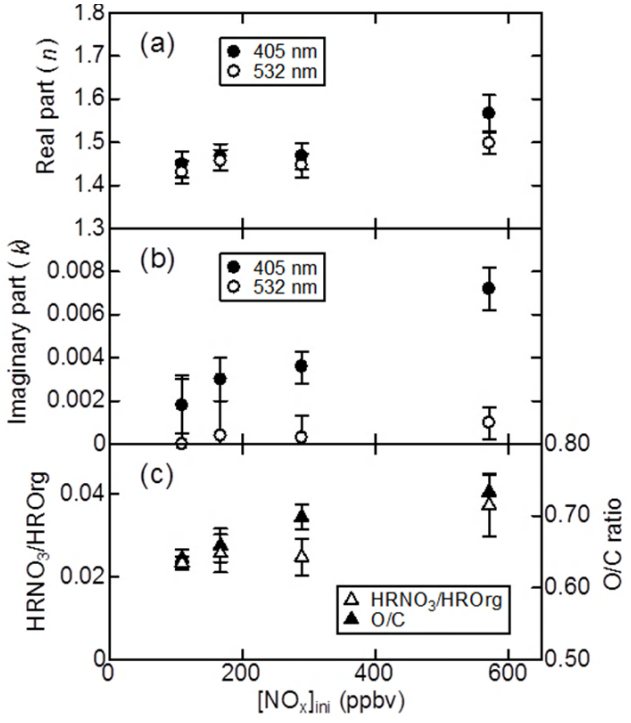


**Fig. 6.** $[NO_x]_{ini}$ dependence of the **(a)** real and **(b)** imaginary parts of the RI-values at 405 and 532 nm for the toluene-SOAs and **(c)** $HRNO_3$/HROrg and O/C ratios measured using H-TOF-AMS. Error bars for the $n$ and $k$-values indicate the uncertainties estimated from the $2\sigma$ values for the differences in the $Q^*$ values obtained using Eqs. (1) and (2) and those in the measurements of the optical properties and size distributions of the SOAs, while those in the $HRNO_3$/HROrg and O/C ratios indicate the $1\sigma$ values of the ratios during the periods used for determination of the RI-values.

(571 ppbv). Because no significant $k$-values at 532 nm were observed under the other $[NO_x]_{ini}$ conditions, it is difficult to discuss the $[NO_x]_{ini}$ dependence of the $k$-value based on these results.

As a plausible source of light-absorption for the toluene-SOAs, nitroaromatic compounds, particularly nitrocresols, have been proposed (Nakayama et al., 2010a; Zhong and Jang 2011), because nitrocresols such as 4-nitro-*o*-cresol, 4-nitro-*m*-cresol, 2-nitro-*p*-cresol, and 4,6-dinitro-*o*-cresol, which were identified as products of toluene-SOAs (Jang and Kamens, 2001; Sato et al., 2007), exhibit strong light absorption at >350 nm (Jacobson, 1999; Chen et al., 2011).

Figure 7 shows one of the significant reaction schemes for the formation of nitrocresols during the photooxidation of toluene in the presence of $NO_x$. There are two steps in the reaction of toluene with OH: abstraction of a H from toluene (∼10 %), and formation of a toluene-OH adduct (∼90 %). The toluene-OH adduct reacts with $O_2$ or $NO_2$, and subsequent reactions of the corresponding products lead to SOA formation. Under our experimental conditions, most of the toluene-OH adduct reacts with $O_2$, while only a few percent of the adduct reacts with $NO_2$ (Koch et al., 2007 and references therein). Although cresols (*o*-, *m*-, *p*-cresol) can be generated from both of these reactions, the cresols are considered to be mainly generated from the reaction of the toluene-OH adduct with $O_2$, because the yields of *o*-, *m*-, and *p*-cresol are reported to be ∼0.12, ∼0.03, and ∼0.03, respectively, and do not strongly depend on the initial $NO_x$ conditions (Smith et al., 1998; Klotz et al., 1998). The H atom abstraction from cresols by OH or $NO_3$ leads to the formation of methyl phenoxy radicals. Nitrocresols are considered to be mainly generated from the reactions of methyl phenoxy radicals with $NO_2$, as shown in Fig. 7 (Forstner et al., 1997; Sato et al., 2007).

The reaction of the cresol-OH adducts with $NO_2$ possibly contributes to the formation of nitrocresols. However, the contribution should be small because most of the cresol-OH adducts react with $O_2$ rather than $NO_2$ (Koch et al., 2007). The fact that the yields of nitrocresols in the OH-induced oxidation of cresols are similar to the calculated fraction of the reaction proceeding via H atom abstraction from the OH group indicates that the nitrocresols are mainly generated through methyl phenoxy radicals (Atkinson et al., 1992; Olariu et al., 2002; Coeur-Tourneur et al., 2006). It should also be noted that nitrotoluenes, such as 3-nitrotoluene, are generated through the reaction of toluene-OH adducts with $NO_2$, particularly at high $[NO_x]_{ini}$ conditions (typically >1 ppm) (Forstner et al., 1997; Smith et al., 1998; Sato et al., 2007). The contribution of nitrotoluenes to the light absorption of the toluene-SOAs should be minimal, however, because both the yield and absorption cross section of nitrotoluenes have been estimated to be smaller than those of nitrocresols under our experimental conditions (Forstner et al., 1997; Smith et al., 1998; Sato et al., 2007; Shama, 1991; Chen et al., 2011).

The observed $[NO_x]_{ini}$ dependence of the $k$-values may be explained by competition reactions of the methyl phenoxy radicals with $NO_2$ and other oxidants, as shown in Fig. 7. Although the rate constants for the reactions of the methyl phenoxy radicals with $NO_2$ and other oxidants are not available, those for the reactions of phenoxy radical ($C_6H_5O$) with $NO_2$, NO, and $O_3$ were reported to be $k_{NO_2} = 2.1 \times 10^{-12}$ (Platz et al., 1998), $k_{NO} = 1.88 \times 10^{-12}$ (Platz et al., 1998), and $k_{O3} = 2.86 \times 10^{-13}$ (Tao and Li, 1999) $cm^3 molecule^{-1} s^{-1}$ at room temperature (296-298 K), respectively. The reaction of the phenoxy radical with $O_2$ was reported to be negligible (Platz et al., 1998). Although possible contributions of the reactions of the phenoxy radical with $HO_2$ and alkylperoxy ($RO_2$) radical cannot be ruled out, the rate constants for these reactions are not available. Assuming that the rate constants for methyl phenoxy radicals are similar to those for the phenoxy radical, and that the reactions with $HO_2$ and $RO_2$ are negligible, the effective yield of the reaction of methyl phenoxy radicals with $NO_2$ ($Y_{NO_2}$) is

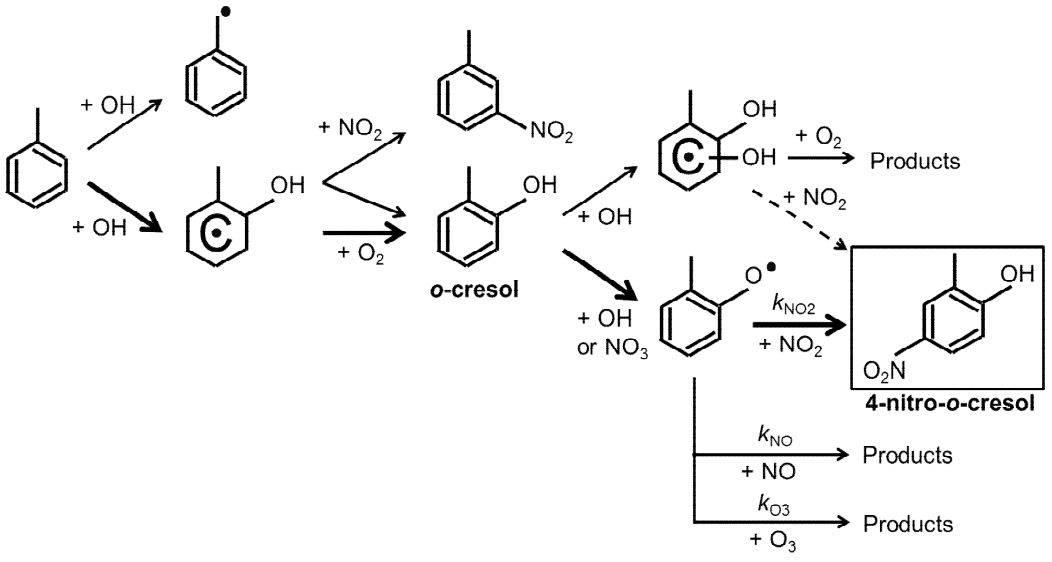


**Fig. 7.** One of the significant reaction schemes for the formation of nitrocresols during photooxidation of toluene in the presence of $NO_x$. The bold arrows indicate the major reaction paths leading to formation of 4-nitro-*o*-cresol under our experimental conditions.

estimated by the following equation:

$$Y_{NO_2} = \frac{k_{NO_2}[NO_2]_{eff}}{k_{NO_2}[NO_2]_{eff} + k_{NO}[NO]_{eff} + k_{O_3}[O_3]_{eff},} \quad (3)$$

where $[NO_2]_{eff}$, $[NO]_{eff}$, and $[O_3]_{eff}$ are the effective concentrations of $NO_2$, NO, and $O_3$, respectively, during the formation of the SOAs. The values for $[NO_2]_{eff}$, $[NO]_{eff}$, and $[O_3]_{eff}$ are calculated using the following equation:

$$[X]_{eff} = \frac{\int_{t_0}^{t_{max}} [X]_t \Delta M_t \, dt}{\int_{t_0}^{t_{max}} \Delta M_t \, dt} (X = NO_2, NO, O_3), \quad (4)$$

where $t_0$ and $t_{max}$ are the time when the irradiation began and when the volume (mass) concentration of the SOAs, which was measured by the SMPS, reached a maximum, respectively; $[X]_t$ is the concentration of X at time $t$; and $\Delta M_t$ is the change in mass concentration of the SOAs during time $dt$. The value of $[X]_{eff}$ is identical to the average concentration of X weighted with the change in mass concentration of the SOAs during the period ($t_0 < t < t_{max}$). The estimated $Y_{NO_2}$ values, along with the values for $[NO_2]_{eff}$, $[NO]_{eff}$, and $[O_3]_{eff}$, are listed in Table 3 for each experimental run. As a result, $Y_{NO_2}$ was found to increase with increasing $[NO_x]_{ini}$. The observed $[NO_x]_{ini}$ dependence of the $k$-values is consistent with the hypothesis that nitrocresols, which are generated through the mechanism described above, are the main contributors to the light absorption of the SOAs. The observed $[NO_x]_{ini}$ dependence of the RI-values was compared with the chemical properties of the SOAs, which were simultaneously measured using H-TOF-AMS. The ratio averages ($\pm 1\sigma$) of the nitrate to the organics ($HRNO_3$/HROrg) and the oxygen atoms to the carbon atoms (O/C) calculated from the H-ToF-AMS data for the same period used for determination of the RI-values are listed in Table 3. The $HRNO_3$/HROrg ratio increases with an increase in the $[NO_x]_{ini}$ from 0.023 to 0.037, as shown in Fig. 6c with the open triangles. Particulate nitroaromatic compounds are known to be detected as nitrate by AMS (Bahreni et al., 2005; Sato et al., 2010, 2012).

It should be noted that the mass concentration of the SOAs may also contribute to the $HRNO_3$/HROrg ratio, since the mass concentration increases with an increase in the $[NO_x]_{ini}$ under the present experimental conditions with a constant $[HC]_{ini}$, as shown in Table 1. Sato et al. (2012) reported that the $HRNO_3$/HROrg ratio for the SOAs generated from the photooxidation of benzene in the presence of $NO_x$ (denoted by benzene-SOAs) was not dependent on the mass loading, but closely dependent on the $[NO_x]_{ini}$. Therefore, the AMS data reinforce the hypothesis that the nitroaromatics, including nitrocresols, contribute to the observed light absorption. The average of the O/C ratio was also found to increase with increasing $[NO_x]_{ini}$ from 0.64 to 0.73, as shown in Fig. 6c with the filled triangles. This result suggests that the oxidation processes of the precursors may also contribute to the enhancement of the light absorption of the toluene-SOAs. The O/C ratios obtained in the present study are roughly consistent with those reported in the literature (e.g., Chhabra et al., 2011; Sato et al., 2012).

### 4.3 RI-values of 1,3,5-TMB-SOAs

The RI-values of 1,3,5-TMB-SOAs were also determined in order to investigate the influence of the chemical structure of the aromatic hydrocarbons on the optical properties of the SOAs. The RI-values of 1,3,5-TMB at 405, 532, and 781 nm were determined to be $1.485^{+0.062}_{-0.054}$-$0.0002^{+0.0004}_{-0.0002}i$,

**Table 3.** Effective concentrations of $NO_2$, NO, and $O_3$ during SOA formation and the chemical properties of the SOAs.

| Run | $[NO_2]^a_{eff}$ (ppbv) | $[NO]^a_{eff}$ (ppbv) | $[O_3]^a_{eff}$ (ppbv) | $Y_{NO_2}$ [b] | $HRNO_3$/HROrg [c] | O/C [c] |
|---|---|---|---|---|---|---|
| A1 | 13 | 0.7 | 178 | 0.34 | $0.023 \pm 0.002$ | $0.64 \pm 0.01$ |
| A2 | 20 | 0.4 | 205 | 0.41 | $0.026 \pm 0.005$ | $0.66 \pm 0.02$ |
| A3 | 45 | 1.9 | 261 | 0.55 | $0.025 \pm 0.004$ | $0.70 \pm 0.02$ |
| A4 | 97 | 2.5 | 301 | 0.69 | $0.037 \pm 0.008$ | $0.73 \pm 0.02$ |
| B1 | 43 | 1.1 | 277 | – | $0.019 \pm 0.001$ | $0.49 \pm 0.01$ |

[a] Effective $NO_2$, NO, and $O_3$ concentrations during the SOA formation, which were estimated using Eq. (4), see text for details.
[b] Effective yield of the methyl phenoxy radials with $NO_2$ during the SOA formation, which were estimated using Eq. (3), see text for details.
[c] Average ($\pm 1\sigma$) of the $HRNO_3$/HROrg and O/C ratios of the SOAs measured by the H-ToF-AMS during the periods used for the determination of the RI-values.

$1.459^{+0.028}_{-0.029}$-$0.0000^{+0.0010}_{-0.0000}i$, and $1.423^{+0.028}_{-0.027}$-$0.0002^{+0.0007}_{-0.0002}i$, respectively, under high $[NO_x]_{ini}$ conditions ($[NO_x]_{ini} =$ 571 ppbv). The $n$-value slightly increased to shorter wavelengths in a manner similar to that observed for the toluene-SOAs. In contrast to the toluene-SOAs, however, the $k$ values for 1,3,5-TMB were found to be negligible at all of the wavelengths studied (405, 532, and 781 nm). The averages ($\pm 1\sigma$) of the $HRNO_3$/HROrg and O/C ratios during the same period as that used for determination of the RI-values were 0.019 $\pm 0.001$ and $0.49 \pm 0.01$, respectively (Table 3). These values are lower than those for the toluene-SOAs (0.023–0.037 ($HRNO_3$/HROrg) and 0.64–0.73 (O/C)) obtained under conditions where the $[NO_x]_{ini}$ was between 109 and 571 ppbv.

In 1,3,5-TMB, the hydrogen atoms in the two *meta* positions to the methyl group in toluene are substituted by other methyl groups. The difference in the light absorption properties between toluene-SOAs and 1,3,5-TMB-SOAs may be explained by the difference in the production of nitrophenols. Sato et al. (2012) compared the chemical properties of the 1,3,5-TMB-SOAs with the benzene-SOAs based on H-ToF-AMS and liquid chromatography/time of flight mass spectrometry (LC/TOF-MS) analyses. They reported that nitrophenols were not detected in the 1,3,5-TMB-SOAs, while they were detected in the benzene-SOAs, and that the $HRNO_3$/HROrg ratio for 1,3,5-TMB was lower than that for the benzene-SOAs and not dependent on the $[NO_x]_{ini}$. These results were explained by the instability of the $NO_2$ adducts of the phenoxy-type radicals produced from 2,4,6-trimethyphenol, which was formed from the reaction of 1,3,5-TMB with OH (Sato et al., 2012). In the resonance structures of the phenoxy-type radicals, the carbon atoms at the radical's center are bonded with methyl groups, and therefore the $NO_2$ adducts of the phenoxy-type radicals immediately dissociate to reactants again (Sato et al., 2012). The fact that no light absorption was revealed for the 1,3,5-TMB-SOAs in the present study is consistent with the hypothesis that nitroaromatics such as nitrocresols are the main sources of the light absorption for the toluene-SOAs. The non-zero $HRNO_3$/HROrg ratio observed in the present study may be due to the contributions of nitrate and nitrite compounds other than nitroaromatics to the $HRNO_3$ signals.

In the case of many other aromatic hydrocarbons, such as benzene, *o*-xylene, *m*-xylene, *p*-xylene, 1,2,4-TMB, and ethylbenzene, there are other meta sites for which the hydrogen atom is not substituted by an alkyl group. Therefore, the photooxidation products of these precursors include stable $NO_2$ adducts of phenoxy-type radicals, and the SOAs generated from these precursors presumably contain nitrophenols and exhibit light absorption at UV and shorter visible wavelengths.

## 5 Atmospheric implications

To estimate the possible contribution of light absorption by the toluene-SOAs, mass absorption cross sections (MACs) at 405 nm were calculated using the obtained RI-values.

If the nitrocresols generated from the methyl phenoxy radicals with $NO_2$ are the main sources of light absorption of the toluene-SOAs, and the yield of the methyl phenoxy radicals is constant, as discussed in Sect. 4.2, then the $k$-values at 405 nm can be considered to be proportional to $Y_{NO_2}$:

$$k(405\,\text{nm}) = A(405\,\text{nm}) \times Y_{NO_2} = A(405\,\text{nm}) \times \frac{k_{NO_2}[NO_2]_{eff}}{k_{NO_2}[NO_2]_{eff} + k_{NO}[NO]_{eff} + k_{O_3}[O_3]_{eff},} \quad (5)$$

where $A(405\,\text{nm})$ is the factor that is proportional to the effective absorption cross section of the light-absorbing species (i.e., nitrocresols). Because $[NO]_{eff}$ is smaller than both $[NO_2]_{eff}$ and $[O_3]_{eff}$ under our experimental conditions, the observed $k(405\,\text{nm})$ values of the SOAs are substantially determined by the ratio of $[NO_2]_{eff}$ to $[O_3]_{eff}$ during SOA formation. Figure 8b shows the $[NO_2]_{eff}/[O_3]_{eff}$ ratio dependence of the $k(405\,\text{nm})$ values for the toluene-SOAs. Minimizing the sum of the squared residual between the measured $k$-values and those calculated using Eq. (5), the $A(405\,\text{nm})$ value was determined to be $0.0083^{+0.0021}_{-0.0021}$. The quoted uncertainties include $2\sigma$ for the differences between the observed

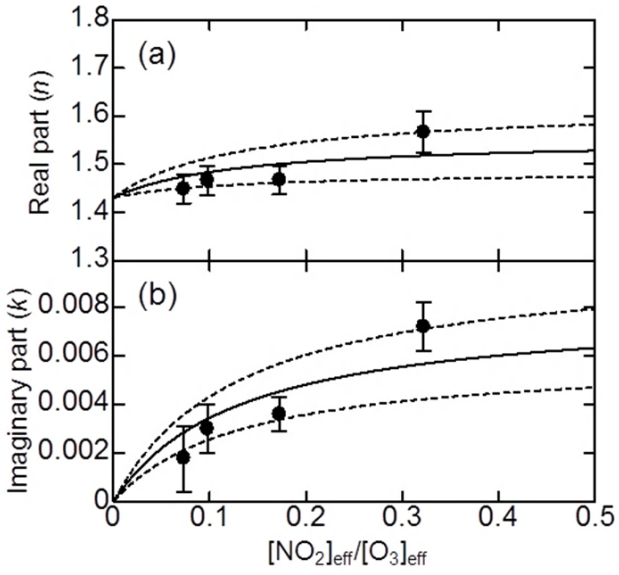


**Fig. 8.** $[NO_2]_{eff}/[O_3]_{eff}$ dependence of the **(a)** real and **(b)** imaginary parts of the RI-values at 405 nm for the toluene-SOAs. The solid and dashed lines are the best estimation and upper (or lower) limit values, respectively, calculated using Eqs. (5) and (6) assuming a constant $[NO]_{eff}/[NO_2]_{eff}$ (=0.04); see text.

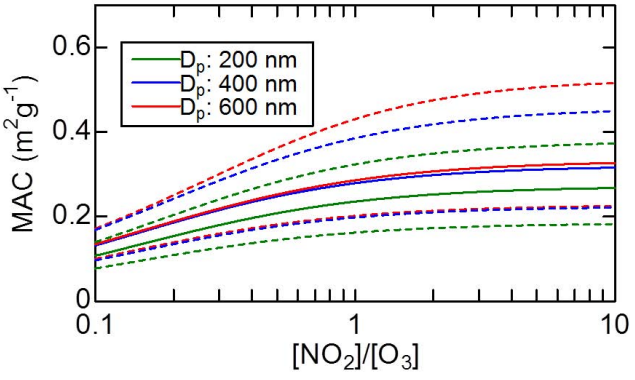


**Fig. 9.** $[NO_2]/[O_3]$ dependence of the MAC values at 405 nm for the toluene-SOAs with particle diameters of 200, 400, and 600 nm, assuming a constant $[NO]/[NO_2]$ (=0.04). The solid and dashed lines are the best estimation and upper (or lower) limit values, respectively.

$k$-values and those calculated using Eq. (5) and the uncertainties in the experimentally determined $k$values.

The $n$values at 405 nm slightly depend on $[NO_2]_{eff}/[O_3]_{eff}$, as shown in Fig. 8a, possibly due to their contribution to the light absorption, as discussed in Sect. 4.2. Assuming that the $n$(532 nm) value obtained under low $[NO_x]_{ini}$ conditions (run A1), 1.431, is a typical $n$-value for the toluene-SOAs without light absorption, the $[NO_2]_{eff}/[O_3]_{eff}$ dependence of the $n$(405 nm) values can be estimated using the following equation:

$$n(405\,\text{nm}) = 1.431 + B(405\,\text{nm}) \times Y_{NO_2} = 1.431 + B(405\,\text{nm}) \times \frac{k_{NO_2}[NO_2]_{eff}}{k_{NO_2}[NO_2]_{eff} + k_{NO}[NO]_{eff} + k_{O_3}[O_3]_{eff}}, \quad (6)$$

where B(405 nm) is the factor that is proportional to the contribution of the light-absorbing species to $n$. Minimizing the sum of the squared residual between the measured $n$-values and those calculated using Eq. (6), the B(405 nm) value was determined to be $0.13^{+0.07}_{-0.07}$. The quoted uncertainties include $2\sigma$ for the differences between the observed $n$-values and those calculated using Eq. (6) and the uncertainties in the experimentally determined $n$-values. The solid (dashed) lines in Fig. 8a and b show the best estimation (and upper or lower limit) values for $n$(405 nm) and $k$(405 nm) calculated using Eqs. (5) and (6) with the optimized $A$(405 nm) and $B$(405 nm) values, respectively, assuming a constant $[NO]_{eff}/[NO_2]_{eff}$ value of 0.04, which is the average for the experimental runs (A1–A4).

Using the obtained $[NO_2]_{eff}/[O_3]_{eff}$-dependent $n$- and $k$-values, the MAC values of the toluene-SOAs at 405 nm were estimated based on Mie theory (BHMIE algorithm) assuming homogeneous spherical particles with a particle density of 1.4 g cm$^{-3}$ (Sato et al., 2007) and a constant $[NO_2]/[O_3]$ ratio during the formation of the SOAs. Usually, [NO] is significantly smaller than $[NO_2]$ during the daytime, when the photooxidation of toluene occurs, because of the rapid conversion of NO to $NO_2$ via reaction with $O_3$. Therefore, a constant $[NO]/[NO_2]$ ratio (=0.04) was assumed in the calculation. Figure 9 shows the $[NO_2]/[O_3]$ dependence of the MACs of the SOAs with diameters of 200, 400, and 600 nm for the typical $[NO_2]/[O_3]$ range between 0.1 and 10 in an urban atmosphere during the daytime (e.g., Finlayson-Pitts and Pitts, 2000; Kondo et al., 2008). The ranges of the best estimates (upper and lower limits) of the MAC values at 405 nm for the toluene-SOAs with diameters between 200 and 600 nm were estimated to be 0.11–0.33 (0.08–0.52) m$^2$g$^{-1}$, respectively. As shown in Fig. 9, the MAC values at 405 nm increase 2.4 times on average with an increase in the $[NO_2]/[O_3]$ ratio from 0.1 to 10, and increase 1.2 times on average with an increase in the particle diameter from 200 to 600 nm.

Several observational studies on the wavelength dependence of the MAC values of brown carbon in urban aerosols (Barnard et al., 2008; Flowers et al., 2010; Zhang et al., 2011; Cheng et al., 2011) have been reported. Barnard et al. (2008) determined the MAC values at wavelengths between 300 and 500 nm for organic components of aerosols in Mexico City, and reported that the MAC steeply decreased from ∼6 m$^2$g$^{-1}$ at 390 nm to ∼1 m$^2$g$^{-1}$ at 410 nm. Flowers et al. (2010) reported that the MAC values for organic carbon in various Asian pollution plumes that were transported to Jeju, Korea ranged between 2.1 and 3.4 m$^2$g$^{-1}$C at 405 nm. The MAC value at 405 nm for the toluene-SOAs obtained in the present study (0.08–0.52 m$^2$g$^{-1}$) is several

times smaller than these reported values. The difference may be explained by contributions of other sources of brown carbon, such as biomass burning, because the reported MAC values for combustion-related organic aerosols (combustion-OA) are typically larger than those for water soluble organic carbons (WSOC) (Sun et al., 2007 and references therein).

Very recently, SOAs generated from anthropogenic VOCs were reported to contribute to the light absorption of WSOC at near UV wavelengths (Zhang et al., 2011; Cheng et al., 2011). Zhang et al. (2011) compared the light absorption spectra of WSOC in the Los-Angeles basin (LA) and Atlanta during the summer, and reported a 4–6 times higher bulk absorption per soluble carbon mass at 365 nm ($\alpha(365\,\mathrm{nm})/\rho$; $\alpha$ is the bulk absorption coefficient, $\rho$ is the density of the WSOC) in LA: (0.69 (weekdays) and 0.77 $\mathrm{m^2 g^{-1}C}$ (weekends)) compared to those in Atlanta. They suggested that the light absorption observed in LA was due to freshly-formed anthropogenic SOAs, because the radio carbon analysis showed that the SOAs were mainly formed by fossil carbon, and the chemical analysis showed a positive correlation between the bulk absorption coefficients with nitroaromatics in the WSOC. The bulk absorption per soluble carbon can be compared with the particulate absorption coefficients using the MAC (Bohren and Hoffman, 1983):

$$\mathrm{MAC} = \frac{6\pi}{\rho\lambda}\mathrm{Im}\left\{\frac{m^2-1}{m^2+2}\right\}\left[1-\frac{4\pi D_P^3}{3\lambda^3}\mathrm{Im}\left\{\frac{m^2-1}{m^2+2}\right\}^2\right]. \quad (7)$$

For particles with $D_p$ <600 nm and $k$ <0.01 at $\lambda$ =405 nm, the term $(4\pi D_p^3/3)\mathrm{Im}\{(m^2\text{-}1)/(m^2\text{+}2)\}^2$ is less than 0.001. Therefore, the MAC is approximated by

$$\mathrm{MAC} = \frac{6\pi}{\rho\lambda}\mathrm{Im}\left\{\frac{m^2-1}{m^2+2}\right\}. \quad (8)$$

As shown by Sun et al. (2007), by expanding the term in brackets and substituting for $\alpha$, the MAC can be related to the bulk absorption:

$$\mathrm{MAC} = \xi \times \alpha/\rho, \quad (9)$$

where $\xi$ is defined by:

$$\xi = \frac{9n}{\left(n^2-k^2+2\right)^2+4n^2k^2}. \quad (10)$$

Applying the $n$(405 nm) and $k$(405 nm) values estimated using Eqs. (5) and (6) for $[NO_2]/[O_3]$ ratios from 0.1 to 10, the $\xi$ values were estimated to be 0.69–0.77. The MAC values at 405 nm were then estimated from the reported $\alpha(365\,\mathrm{nm})/\rho$ values to be 0.30–0.48 $\mathrm{m^2 g^{-1}C}$ using a mean absorption Ångström exponent (AAE) of $3.2 \pm 1.2$ for LA and the $\xi$ values, because Zhang et al. (2011) reported a linear relationship between $\log(b_{\mathrm{abs}})$ and $\log(\lambda)$ in this wavelength range. The ranges of the best estimates (upper and lower limits) of the MAC values at 405 nm for the toluene-SOAs with diameters between 200–600 nm estimated in the present study, 0.11–0.33 (0.08–0.52) $\mathrm{m^2 g^{-1}}$, were converted to those per carbon mass, 0.22–0.69 (0.16–1.09) $\mathrm{m^2 g^{-1}C}$, by taking into account the range of the O/C, H/C, and N/C ratios measured via ToF-AMS during "runs A1–A4". These values are roughly consistent with the MAC values at 405 nm estimated based on the observations in LA by Zhang et al. (2011) (0.30–0.48 $\mathrm{m^2 g^{-1}C}$), although it should be noted that the wavelength dependence of light absorption for the toluene-SOAs and the particles observed in LA may be different.

The typical MAC values at 405 nm for the BC particles were estimated to be 10.2 $\mathrm{m^2 g^{-1}}$ from the value reported by Bond and Bergstrom (2006), assuming an AAE of 1. The estimated MAC values for BC are 30–90 (20–130) times larger than the best estimates (upper and lower limits) of the MAC values determined in this study for the toluene-SOAs at 405 nm. However, the temporal and spatial variations of the relative abundance of BC and anthropogenic SOAs should be large. Therefore, the light absorption by the anthropogenic SOAs potentially contributes to the radiation balance at UV wavelengths below ~400 nm, specifically when the relative abundance of the anthropogenic SOAs is significant.

It should be noted that the mass concentrations of the toluene-SOAs generated in the present study were higher than typical atmospheric organic mass loadings (0.1–20 $\mu\mathrm{g\,m^{-3}}$). Although the contribution of the mass loading to the optical properties would be small under our experimental conditions as discussed in Sect. 4.2, a possible contribution of the mass loading under atmospheric conditions cannot be ruled out. The relative abundance of a chemical compound mainly depends on the vapor pressures of the chemical compounds comprising the SOAs (e.g., Donahue et al., 2006, Shilling et al., 2009). The vapor pressures of nitrocresols range from $1 \times 10^{-5}$ to $2 \times 10^{-2}$ Torr (Heintz et al., 2007), and correspond to mass-equivalent effective saturation concentrations from $1 \times 10^2$ to $3 \times 10^5 \mu\mathrm{g\,m^{-3}}$ when an activity coefficient of 1 and an average molecular weight for the SOAs of 250 g $\mathrm{mol^{-1}}$ are assumed (Donahue et al., 2006). If the vapor pressures of non-light-absorbing compounds in the toluene-SOAs are significantly lower than those of light-absorbing compounds such as nitrocresols, the relative abundance of the light absorbing compounds in the SOAs, and therefore the MAC values at 405 nm, might be lower under atmospheric conditions. It should also be noted that the reaction of cresols with $NO_3$ possibly contributes to the formation of nitrocresols, because these reactions are considered to produce phenoxy radicals efficiently, and then the phenoxy radicals react with $NO_2$ to form nitrocresols (Atkinson et al., 1992; Klotz et al., 1998; Calvert et al., 2002). Because the rate constants for the reactions of cresols with $NO_3$ are 1/3–1/8 of those with OH at room temperature (Atkinson et al., 1992), the competition reactions of cresols with $NO_3$ and OH would also contribute to the yield of nitrocresols if the $[NO_3]$

was higher than the [OH] during the formation of SOAs under our experimental conditions. In this case, the yield of nitrocresols produced in the atmosphere during the daytime may be lower. In addition, the presence of seed particles may enhance the light absorption of the toluene-SOAs by a factor of 2–3, as reported by Zhong and Jang (2011). Therefore, further studies on the contribution of other possible factors, such as the presence of seed particles, the initial VOC concentrations (mass loading), and the generation of SOAs from other anthropogenic VOCs and reactants, to the RI values of SOAs are needed.

## 6 Conclusions

In the present study, the $[NO_x]_{ini}$ dependence of the complex RI-values at 405, 532, and 781 nm for toluene-SOAs was determined. The imaginary part of the RI-value ($k$) for toluene-SOAs was found to increase to shorter wavelengths at $<$532 nm, and the real part of the RI-value ($n$) also increased to shorter wavelengths from 781 to 355 nm. The $k$-value at 405 nm was found to increase from 0.0018 to 0.0072 with increasing $[NO_x]_{ini}$ from 109 to 571 ppbv. The $HRNO_3$/HROrg and O/C ratios of the SOAs determined using H-ToF-AMS also increased with increasing $[NO_x]_{ini}$. Our results imply that nitroaromatic compounds, probably nitrocresols, are the main cause of light absorption by toluene-SOAs, and that oxidation processes of the precursors may also contribute to the enhancement of the light absorption of toluene-SOAs. The RI-values of the 1,3,5-TMB-SOAs generated under a high $[NO_x]_{ini}$ condition were also determined for the first time. The light absorption of the 1,3,5-TMB-SOAs was found to be negligible at all wavelengths (405, 532, and 781 nm). These results are explained by suppression of the formation of nitrophenols due to the instability of the $NO_2$ adducts of the phenoxy-type radicals produced from 2,4,6-trimethylphenol, which was formed from the reaction of 1,3,5-TMB with OH.

Using the obtained RI-values, the MACs of the toluene-SOAs at 405 nm were estimated to be 0.08–0.52 $m^2 g^{-1}$, under typical conditions in urban atmospheres during the daytime. These results indicate that light absorption by the SOAs potentially contributes to the radiation balance at UV wavelengths below $\sim$400 nm, specifically when the relative abundance of the anthropogenic SOAs is significant compared with other light-absorbing particles. The estimated MAC values at 405 nm for the toluene-SOAs are roughly consistent with those estimated based on the bulk light absorption of WSOC observed in LA by Zhang et al. (2011).

This study suggests that the optical properties of SOAs generated from aromatic hydrocarbons depend on the concentration of $NO_x$ and $O_3$ during SOA formation, as well as the chemical structures of the precursors. Therefore, further studies of the optical properties of SOAs generated from a variety of aromatic hydrocarbons (including their isomers) and their $[NO_x]_{ini}$ dependence are required for a precise understanding of the atmospheric implications of light-absorbing anthropogenic SOAs. In addition, further experimental studies of these SOAs at shorter wavelengths (e.g., $<$330 nm) are also desired in order to evaluate the influence of particle absorption on photochemistry in the atmosphere by varying the photolysis rate of $O_3$.

**Supplementary material related to this article is available online at: http://www.atmos-chem-phys.net/13/531/2013/acp-13-531-2013-supplement.pdf.**

*Acknowledgements.* We would like to thank Y. Goto and Y. Ikeda (Nagoya Univ.) for their assistance with the experiments. This study was supported by the global environmental research fund of the Japanese Ministry of the Environment (RF-1008), the Ministry of Education, Culture, Sports, Science and Technology (MEXT) (KAKENHI 20120007, 21710007, 22310015), the Steel Foundation for Environmental Protection Technology, and the joint research program of the Solar-Terrestrial Environment Laboratory, Nagoya University.

Edited by: R. Volkamer

## References

Adler, G., Abo Riziq, A., Erlick, C., and Rudich, Y.: Effect of intrinsic organic carbon on the optical properties of fresh diesel soot, Proc. Natl. Acad. Sci. USA, 107, 6699–6704, 2010.

Akimoto, H., Hoshino, H., Inoue, G., Sakamaki, F., Washida, N., and Okuda, M.: Design and characterization of the evacuable and bankable photochemical smog chamber, Environ. Sci. Technol., 13, 471-475, 1979.

Alexander, D. T. L., Crozier, P. A., and Anderson, J. R.: Brown carbon spheres in east Asian outflow and their optical properties, Science, 321, 833–836, 2008.

Andreae, M. O. and Gelencsér, A.: Black carbon or brown carbon? The nature of light-absorbing carbonaceous aerosols, Atmos. Chem. Phys., 6, 3131–3148, doi:10.5194/acp-6-3131-2006, 2006.

Atkinson, R., Aschmann, S. M., and Arey, J.: Reactions of OH and $NO_3$ radicals with phenol, cresols, and 2-nitrophenol, at 296 $\pm$2 K, Environ. Sci. Technol. 26, 1397–1403, 1992.

Barnard, J. C., Volkamer, R., and Kassianov, E. I.: Estimation of the mass absorption cross section of the organic carbon component of aerosols in the Mexico City Metropolitan Area, Atmos. Chem. Phys., 8, 6665–6679, doi:10.5194/acp-8-6665-2008, 2008.

Bahreini, R., Keywood, M. D., Ng, N. L., Varutbangkul, V., Gao, S., Flagan, R. C., Seinfeld, J. H., Worsnop, D. R., Jimenez, J. L.: Measurements of secondary organic aerosol from oxidation of cycloalkenes, terpenes, and $m$-xylene using an Aerodyne aerosol mass spectrometer, Environ. Sci. Technol., 39, 5674–5688, 2005.

Bohren, C. F. and Huffman, D. R.: Absorption and scattering of light by small particles, John-Wiley & Sons. Inc., New York, USA, 1983.

Bond, T.: Spectral dependence of visible light absorption by carbonaceous particles emitted from coal combustion, Geophys. Res. Lett., 28, 4075–4078, 2001.

Bond, T. C. and Bergstrom, R. W.: Light absorption by carbonaceous particles: An investigative review, Aerosol Sci. Technol., 40, 27–67, 2006.

Bones, D. L., Henricksen, D. K., Mang, S. A., Gonsior, M., Bateman, A. P., Nguyen, T. B., Cooper, W. J., and Nizkorodov, S. A.: Appearance of strong absorbers and fluorophores in limonene-$O_3$ secondary organic aerosol due to $NH_4^+$-mediated chemical aging over long time scales, J. Geophys. Res., 115, D05203, doi:10.1029/2009JD012864, 2010.

Calvert, J. K., Atkinson, R., Becker, K. H., Kamens, R. M., Seinfeld, J. H., Wallington, T. J., and Yarwood, G.: The mechanism of atmospheric oxidation of aromatic hydrocarbons, Oxford Univ. Press, New York, USA, 2002.

Cappa, C. D., Che, D. L., Kessler, S. H., Kroll, J. H., and Wilson, K. R.: Variations in organic aerosol optical and hygroscopic properties upon heterogeneous OH oxidation, J. Geophys. Res., 116, D15204, doi:10.1029/2011JD015918, 2011.

Chang, J. L. and Thompson, J. E.: Characterization of colored products formed during irradiation of aqueous solutions containing $H_2O_2$ and phenolic compounds, Atmos. Environ., 44, 541–551, 2010.

Chen, Y. and Bond, T.: Light absorption by organic carbon from wood combustion, Atmos. Chem. Phys., 10, 1773-1787, 2010, http://www.atmos-chem-phys.net/10/1773/2010/.

Chen, J., Wenger, J. C., and Venables, D. S.: Near-ultraviolet absorption cross section of nitrophenols and their potential influence on tropospheric oxidation capacity, J. Phys. Chem. A, 115, 12235–12242, 2011.

Cheng, Y., He, K.-B., Zheng, M., Duan, F.-K., Du, Z.-Y., Ma, Y.-L., Tan, J.-H., Yang, F.-M., Liu, J.-M., Zhang, X.-L., Weber, R. J., Bergin, M. H., and Russell, A. G.: Mass absorption efficiency of elemental carbon and water-soluble organic carbon in Beijing, China, Atmos. Chem. Phys., 11, 11497–11510, doi:10.5194/acp-11-11497-2011, 2011.

Chhabra, P. S., Ng, N. L., Canagaratna, M. R., Corrigan, A. L., Russell, L. M., Worsnop, D. R., Flagan, R. C., and Seinfeld, J. H.: Elemental composition and oxidation of chamber organic aerosol, Atmos. Chem. Phys., 11, 8827–8845, doi:10.5194/acp-11-8827-2011, 2011.

Coeur-Tourneur, C., Henry, F., Janquin, M.-A., and Brutier, L.: Gas-phase reaction of hydroxyl radicals with *m*-, *o*- and *p*-cresol, Int. J. Chem. Kinet., 38, 553–562, 2006.

Dinar, E., Abo Riziq, A., Spindler, C., Erlick, C., Kissc, G., and Rudich, Y.: The complex refractive index of atmospheric and model humic-like substances (HULIS) retrieved by a cavity ring down aerosol spectrometer (CRD-AS), Faraday Discuss., 137, 279–295, 2008.

Donahue, N. M., Robinson, A. L., Stanier, C. O., and Pandis, S. N.: The coupled partitioning, dilution, and chemical aging of semivolatile organics, Environ. Sci. Technol., 40, 2635–2643, 2006.

Drewnick, F., Hings, S. S., DeCarlo, P. F., Jayne, J. T., Gonin, M., Fuhrer, K., Weimer, S., Jiminez, J. L., Demerjian, K. L., Borrmann, S., and Worsnop, D. R.: A new time-of-flight aerosol mass spectrometer (ToF-AMS) – instrument description and first field deployment, Aerosol Sci. Tech., 39, 637–658, 2005.

Favez, O., Alfaro, S. C., Sciare, J., Cachier, H., and Abdelwahab, M. M.: Ambient measurements of light-absorption by agricultural waste burning organic aerosols, J. Aerosol Sci., 40, 613–620, 2009.

Finlayson-Piits, B. J. and Pitts Jr., J. N.: Chemistry of the upper and lower atmosphere, Academic Science Press, New York, USA, 2000.

Flowers, B. A., Dubey, M. K., Mazzoleni, C., Stone, E. A., Schauer, J. J., Kim, S.-W., and Yoon, S. C.: Optical-chemical-microphysical relationships and closure studies for mixed carbonaceous aerosols observed at Jeju Island; 3-laser photoacoustic spectrometer, particle sizing, and filter analysis, Atmos. Chem. Phys., 10, 10387–10398, doi:10.5194/acp-10-10387-2010, 2010.

Forstner, H. J. L., Flagan, R. C., and Seinfeld, J. H.: Secondary organic aerosol from the photooxidation of aromatic hydrocarbons: molecular composition, Aerosol Sci. Technol., 31, 1345–1358, 1997.

Galloway, M. M., Chhabra, P. S., Chan, A. W. H., Surratt, J. D., Flagan, R. C., Seinfeld, J. H., Keutsch, F. N.: Glyoxal uptake on ammonium sulphate seed aerosol: reaction products and reversibility of uptake under dark and irradiated conditions, Atmos. Chem. Phys., 9, 3331-3345, 2009, http://www.atmos-chem-phys.net/9/3331/2009/.

Graber, E. R. and Rudich, Y.: Atmospheric HULIS: How humic-like are they? A comprehensive and critical review, Atmos. Chem. Phys., 6, 729–753, doi:10.5194/acp-6-729-2006, 2006.

Hallquist, M., Wenger, J. C., Baltensperger, U., Rudich, Y., Simpson, D., Claeys, M., Dommen, J., Donahue, N. M., George, C., Goldstein, A. H., Hamilton, J. F., Herrmann, H., Hoffmann, T., Iinuma, Y., Jang, M., Jenkin, M. E., Jimenez, J. L., Kiendler-Scharr, A., Maenhaut, W., McFiggans, G., Mentel, Th. F., Monod, A., Prévôt, A. S. H., Seinfeld, J. H., Surratt, J. D., Szmigielski, R., and Wildt, J.: The formation, properties and impact of secondary organic aerosol: current and emerging issues, Atmos. Chem. Phys., 9, 5155–5236, doi:10.5194/acp-9-5155-2009, 2009.

Heintz, A., Kapteina, S., and Verevkin, S. P.: Pairwise-substitution effects and intramolecular hydrogen bonds in nitrophenols and methylnitrophenols. Thermochemical measurements and ab initio calculations, J. Phys. Chem. A, 111, 6552–6562, 2007.

Henze, D. K., Seinfeld, J. H., Ng, N. L., Kroll, J. H., Fu, T.-M., Jacob, D. J., and Heald, C. L.: Global modeling of secondary organic aerosol formation from aromatic hydrocarbons: high- vs. low-yield pathways, Atmos. Chem. Phys., 8, 2405–2420, doi:10.5194/acp-8-2405-2008, 2008.

Hoffer, A., Gelencsér, A., Guyon, P., Kiss, G., Schmid, O., Frank, G. P., Artaxo, P., and Andreae, M. O.: Optical properties of humic-like substances (HULIS) in biomass-burning aerosols, Atmos. Chem. Phys., 6, 3563–3570, doi:10.5194/acp-6-3563-2006, 2006.

Jacobson, M. Z.: Isolating nitrated and aromatic aerosols and nitrated aromatic gases as sources of ultraviolet light absorption, J. Geophys. Res., 104, 3527–3542, 1999.

Jang, M. and Kamens R. M.: Characterization of secondary aerosol from the photooxidation of toluene in the presence of $NO_x$ and 1-propene, Environ. Sci. Technol., 35, 3626–3639, 2001.

Jaoui, M., Edney, E. O., Kleindienst, T. E., Lewandowski, M., Offenberg, J. H., Suratt, J. D., and Seinfeld, J. H.: Formation of secondary organic aerosol from irradiated $\alpha$-pinene/toluene/$NO_x$

mixtures and the effect of isoprene and sulfur dioxide, J. Geophys. Res., 113, D24212, doi:10.1029/2007JD009426, 2008.

Kim, H., Barkey, B., and Paulson, S. E.: Real refractive indices of $\alpha$- and $\beta$-pinene and toluene secondary organic aerosols generated from ozonolysis and photooxidation, J. Geophys. Res., 115, D09303, doi:10.1029/2010JD014549, 2010.

Kirchstetter, T. W., Novakov, T., and Hobbs, P. V.: Evidence that the spectral dependence of light absorption by aerosols is affected by organic carbon, J. Geophys. Res., 109, D21208, doi:10.1029/2004JD004999, 2004.

Kleindienst, T. E., Conver, T. S., McIver, C. D., and Edney, E. O.: Determination of secondary organic aerosol products from the photooxidation of toluene and their implications in ambient $PM_{2.5}$, J. Atmos. Chem., 47, 79–100, 2004.

Klotz, B., Sørensen, S., Barnes, I., Becker, K. H., Etzkorn, T., Volkamer, R., Platt, U., Wirtz, K., and Martín-Reviejo, M.: Atmospheric oxidation of toluene in a large-volume outdoor photoreactor: In situ determination of ring-retaining product yields, J. Phys. Chem. A, 102, 10289–10299, 1998.

Koch, R., Knispel, R., Elend, M., Siese, M., and Zetzsch, C.: Consecutive reactions of aromatic-OH adducts with NO, $NO_2$ and $O_2$: benzene, naphthalene, toluene, m- and p-xylene, hexamethylbenzene, phenol, m-cresol and aniline, Atmos. Chem. Phys., 7, 2057–2071, doi:10.5194/acp-7-2057-2007, 2007.

Kondo, Y., Morino, Y., Fukuda, M., Kanaya, Y., Miyazaki,Y., Takegawa, N., Tanimoto, H., McKenzie, R., Johnston, P., Blake, D. R., Murayama, T., and Koike, M.: Formation and transport of oxidized reactive nitrogen, ozone, and secondary organic aerosol in Tokyo, J. Geophys. Res., 113, D21310, doi:10.1029/2008JD010134, 2008.

Laskin, J., Laskin, A., Roach, P. J., Slysz, G., Anderson, G. A., Nizkorodov, S. A., Bones, D. L., and Nguyen, L. Q.: High-resolution desorption electrospray ionization mass spectrometry for chemical characterization of organic aerosols, Anal. Chem., 82, 2048–2058, 2010.

Milles, R. E., Rudić, S., Orr-Ewing, A. J., and Reid, J.: Influence of uncertainties in the diameter and refractive index of calibration polystyrene beads on the retrieval of aerosol optical properties using cavity ring down spectroscopy, J. Phys. Chem. A, 114, 7077–7084, 2010.

Moosmüller, H., Chakrabarty, R. K., and Arnott, W. P.: Aerosol light absorption and its measurement: A review, J. Quant. Spectrosc. Ra., 110, 844–878, 2009.

Moosmüller, H., Chakrabarty, R. K., Ehlers, K. M., and Arnott, W. P.: Absorption Ångström coefficient, brown carbon, and aerosols: basic concepts, bulk matter, and spherical particles, Atmos. Chem. Phys., 11, 1217–1225, doi:10.5194/acp-11-1217-2011, 2011.

Nakayama, T., Matsumi, Y., Sato, K., Imamura, T., Yamazaki, A., and Uchiyama, A.: Laboratory studies on optical properties of secondary organic aerosols generated during the photooxidation of toluene and the ozonolysis of $\alpha$-pinene, J. Geophys. Res., 115, D24204, doi:10.1029/2010JD014387, 2010a.

Nakayama, T., Hagino, R., Matsumi, Y., Sakamoto, Y., Kawasaki, M., Yamazaki, A., Uchiyama, A., Kudo, R. Moteki, N., Kondo, Y., and Tonokura, K.: Measurements of aerosol optical properties in central Tokyo during summertime using cavity ring-down spectroscopy: Comparison with conventional techniques, Atmos. Environ., 44, 3034–3042, 2010b.

Nakayama, T., Sato, K., Imamura, T., Yamazaki, A., Uchiyama, A., and Matsumi, Y.: Wavelength dependence of refractive index of secondary organic aerosols generated during the ozonolysis and photooxidation of $\alpha$-pinene, SOLA, 8, 119–123, 2012.

Ng, N. L., Kroll, J. H., Chan, A. W. H., Chhabra, P. S., Flagan, R. C., and Seinfeld, J. H.: Secondary organic aerosol formation from *m*-xylene, toluene, and benzene, Atmos. Chem. Phys., 7, 3909–3922, doi:10.5194/acp-7-3909-2007, 2007.

Olariu, R. I., Klotz, B., Barnes, I., Becker, K. H., and Mocanu, R.: FT–IR study of the ring-retaining products from the reaction of OH radicals with phenol, *o*-, *m*-, and *p*-cresol, Atmos. Environ., 36, 3685–3697, 2002.

Platz, J., Nielsen, O. J., Wallington, T. J., Ball, J. C., Hurley, M. D., Straccia, A. M., Schneider, W. F., and Sehested, J.: Atmospheric chemistry of the phenoxy radical, $C_6H_5O(\bullet)$: UV spectrum and kinetics of its reaction with NO, $NO_2$, and $O_2$, J. Phys. Chem. A, 102, 7964–7974, 1998.

Sareen, N., Schwier, A. N., Shapiro, E. L., Mitroo, D., and McNeill, V. F.: Secondary organic material formed by methylglyoxal in aqueous aerosol mimics, Atmos. Chem. Phys., 10, 997–1016, doi:10.5194/acp-10-997-2010, 2010.

Sato, K., Hatakeyama, S., and Imamura, T.: Secondary organic aerosol formation during the photooxidation of toluene: $NO_x$ dependence of chemical composition, J. Phys. Chem., A111, 9796–9808, 2007.

Sato, K., Takami, A., Isozaki, T., Hikida, T., Shimono, A., and Imamura, T.: Mass spectrometric study of secondary organic aerosol formed from the photo-oxidation of aromatic hydrocarbons, Atmos. Environ., 44, 1080–1087, 2010.

Sato, K., Takami, A., Kato, Y., Seta, T., Fujitani, Y., Hikida, T., Shimono, A., and Imamura, T.: AMS and LC/MS analyses of SOA from the photooxidation of benzene and 1,3,5-trimethylbenzene in the presence of $NO_x$: effects of chemical structure on SOA aging, Atmos. Chem. Phys., 12, 4667–4682, doi:10.5194/acp-12-4667-2012, 2012.

Schnaiter, M., Schmid, O., Petzold, A., Fritzsche, L., Klein, K. –F., Andreae, M. O., Helas, G., Thielmann, A., Gimmler, M., Möhler, O., Linke, C., and Schurath, U.: Measurement of wavelength resolved light absorption by aerosols utilizing a UV-VIS extinction cell, Aerosol Sci. Technol., 39, 249–260, 2005.

Schnaiter, M., Gimmler, M., Llamas, I., Linke, C., Jäger, C., and Mutschke, H.: Strong spectral dependence of light absorption by organic carbon particles formed by propane combustion, Atmos. Chem. Phys., 6, 2981–2990, doi:10.5194/acp-6-2981-2006, 2006.

Seinfeld, J. H. and Pandis, S. N.: Atmospheric chemistry and physics: from air pollution to climate change, 2nd edn., Wiley Interscience, New York, 2006.

Shama, S. A.: Vacuum ultraviolet absorption spectra of organic compounds in gaseous and liquid state, Thesis of Faculty of Science, Zagazig University, Egypt, 1991.

Shapiro, E. L., Szprengiel, J., Sareen, N., Jen, C. N., Giordano, M. R., and McNeill, V. F.: Light-absorbing secondary organic material formed by glyoxal in aqueous aerosol mimics, Atmos. Chem. Phys., 9, 2289–2300, doi:10.5194/acp-9-2289-2009, 2009.

Shilling, J. E., Chen, Q., King, S. M., Rosenoern, T., Kroll, J. H., Worsnop, D. R., DeCarlo, P. F., Aiken, A. C., Sueper, D., Jimenez, J. L., and Martin, S. T.: Loading-dependent elemental composition of $\alpha$-pinene SOA particles, Atmos. Chem. Phys., 9,

771–782, doi:10.5194/acp-9-771-2009, 2009.

Smith, D. F., McIver, C. D., and Kleindienst, T. E.: Primary product distribution from the reaction of hydroxyl radicals with toluene at ppb $NO_x$ mixing ratios, J. Atmos. Chem., 30, 209–228, 1998.

Sun, H., Biedermann, L., Bond, T. C.: Color of brown carbon: A model for ultraviolet and visible light absorption by organic carbon aerosol, Geophys. Res. Lett., 34, L17813, doi:10.1029/2007GL029797, 2007.

Tao, Z. N. and Li, Z. J.: A kinetics study on reactions of $C_6H_5O$ with $C_6H_5O$ and $O_3$ at 298 K, Int. J. Chem. Kinet., 31, 65–72, 1999.

Trainic, M., Abo Riziq, A., Lavi, A., Flores, J. M., and Rudich, Y.: The optical, physical and chemical properties of the products of glyoxal uptake on ammonium sulfate seed aerosols, Atmos. Chem. Phys., 11, 9697–9707, doi:10.5194/acp-11-9697-2011, 2011.

Zhang, X., Lin, Y. -H., Surratt, J. D., Zotter, P., Prévôt, A. S. H., and Weber, R. J.: Light-absorbing soluble organic aerosol in Los Angeles and Atlanta: A contrast in secondary organic aerosol, Geophys. Res. Lett., 38, L21810, doi:10.1029/2011GL049385, 2011.

Zhong, M. and Jang, M.: Light absorption coefficient measurement of SOA using a UV-Visible spectrometer connected with an integrating sphere, Atmos. Environ., 45, 4263–4271, 2011.